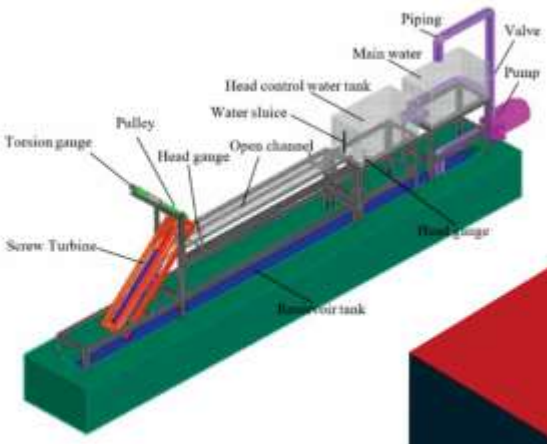

NUMERICAL SIMULATION

ON FREE SURFACE FLOW AROUND A SCREW TURBINE MOVING-PARTICLE SEMI-IMPLICIT METHOD

Dr. Tineke Saroinsong, S.ST., M.Eng.

Numerical Simulation of Free Surface Flow around a Screw Turbine using Moving-Particle Semi-implicit Method

PENULIS
DR. TINEKE SAROINSONG, SST., M.ENG

UU No. 28 Tahun 2014 tentang Hak Cipta

Fungsi dan Sifat Hak Cipta Pasal 4

Hak Cipta sebagaimana dimaksud dalam Pasal 3 huruf a merupakan hak eksklusif yang terdiri atas hak moral dan hak ekonomi.

Pembatasan Pelindungan Pasal 26

Ketentuan sebagaimana dimaksud dalam Pasal 23, Pasal 24, dan Pasal 25 tidak berlaku terhadap:

i. penggunaan kutipan singkat Ciptaan dan/atau produk Hak Terkait untuk pelaporan peristiwa aktual yang ditujukan hanya untuk keperluan penyediaan informasi aktual;
ii. penggandaan Ciptaan dan/atau produk Hak Terkait hanya untuk kepentingan penelitian ilmu pengetahuan;
iii. penggandaan Ciptaan dan/atau produk Hak Terkait hanya untuk keperluan pengajaran, kecuali pertunjukan dan fonogram yang telah dilakukan pengumuman sebagai bahan ajar; dan
iv. penggunaan untuk kepentingan pendidikan dan pengembangan ilmu pengetahuan yang memungkinkan suatu Ciptaan dan/atau produk Hak Terkait dapat digunakan tanpa izin Pelaku Pertunjukan, Produser Fonogram, atau Lembaga Penyiaran.

Sanksi Pelanggaran Pasal 113

1. Setiap orang yang dengan tanpa hak melakukan pelanggaran hak ekonomi sebagaimana dimaksud dalam Pasal 9 ayat (1) huruf i untuk Penggunaan Secara Komersial dipidana dengan pidana penjara paling lama 1 (satu) tahun dan/atau pidana denda paling banyak Rp100.000.000,00 (seratus juta rupiah).
2. Setiap orang yang dengan tanpa hak dan/atau tanpa izin Pencipta atau pemegang Hak Cipta melakukan pelanggaran hak ekonomi Pencipta sebagaimana dimaksud dalam Pasal 9 ayat (1) huruf c, huruf d, huruf f, dan/atau huruf h untuk Penggunaan Secara Komersial dipidana dengan pidana penjara paling lama 3 (tiga) tahun dan/atau pidana denda paling banyak Rp500.000.000,00 (lima ratus juta rupiah).

Numerical Simulation of Free Surface Flow around a Screw Turbine using Moving-Particle Semi-Implicit Method

Dr. Tineke Saroinsong, SST., M.Eng

TATA LETAK:
Wahyuni Putri Adeningsi

DESAIN SAMPUL:
Rachmadiansyah

SUMBER:
www.tangguhdenarajaya.com

ISBN:
978-623-8429-45-5

UKURAN:
iii + 67 Hal; 15.5 cm x 23 cm

CETAKAN PERTAMA:
Oktober 2023

ANGGOTA IKAPI: 006/NTT/2022
PENERBIT TANGGUH DENARA JAYA
Jl. Timor Raya No. 130 B Oesapa Barat, Kelapa Lima
Kota Kupang, Nusa Tenggara Timur
E-mail: tangguhdenarajaya@gmail.com
Telepon: 0380-8436618/081220051382

FOREWORD

I would like to praise the presence of Almighty and All Loving God for His mercy and grace so that the author can complete this monograph with the title " Numerical Simulation of Free Surface Flow around a Screw Turbine using Moving-Particle Semi-implicit Method ".

This monograph is one of the results of my research which is arranged systematically and neatly.The screw turbine is adopted from the Archimedean screw theory which is used as a pump. Seeing the potential for river flows in Indonesia, on average, they have low heads, therefore screw turbines are very suitable for micro-hydro power plants in Indonesia.

The need for energy is the main motivation for energy conversion experts to be able to design or develop various types of tools or energy conversion systems that are environmentally friendly by utilizing energy sources available in nature. One of the energy conversion systems is a screw turbine which is inspired by the workings of an inverted screw pump. The advantage of screw turbines is that they have high slenderness and great rigidity so that the potential for vibration is low due to fluctuations in the flow of water through them. The high rigidity and slenderness of the screw turbine is an advantage/suitability for the application of the free surface flow approach as a method for multi-phase fluid flow analysis with low fluid flow velocity.

Of the many methods for free surface flow analysis, one of which is Moving-Particle Semi-implicit (MPS) which assumes water as a particle moving in a transient condition. The MPS method is used to estimate the performance of a screw turbine with a diameter of 110 mm, a length of 924 mm installed at a slope of 25^0, 35^0 and 45^0 to the ground and driven by water with a mass flow rate of about 1.3 kg/s with a water surface head determined from the length of the turbine and the angle of inclination. The prediction results of screw turbine performance using the MPS method are quite close to the test results with relative error values of 4.76%, 4.36% and 1.52% respectively for turbine positions with slopes of 25^0, 35^0 and 45^0.

The author realizes that this monograph is still far from perfect, so suggestions and criticism are expected from readers to improve the writing process in the future. Hopefully this monograph can provide benefits to readers.

Manado, 14 November 2023

Author

LIST OF CONTENT

FOREWORD ..... **I**

LIST OF CONTENT ..... **III**

BAB 1 INTRODUCTION **1**

BAB 2 EXPERIMEN MODEL **9**

EXPERIMENTAL MODEL 9

BAB 3 NUMERICAL MODEL **15**

PARTICLEWORK CFD CODE 15
GOVERNING EQUATIONS 16
PARTICLE INTERACTION MODEL 17
MODELING TERM 20
ALGORITHM 21
FREE SURFACE CONDITION 23
GRAVITY 24
VISCOSITY 24
RIGID BODY 25
COLLISION AND FRICTION OF PARTICLES 31
SCREW TURBINE GEOMETRY 36

BAB 4 CALCULATION ALGORITHM **40**

BAB 5 PRESSURE **46**

BAB 6 VELOCITY **48**

BAB 7 FREE SURFACE **53**

BAB 8 TURBINE POWER **56**

REFERENCES **61**

BAB 1
INTRODUCTION

The need for energy is the main motivation for energy conversion experts to be able to design or develop various types of tools or energy conversion systems (ECS) that are environmentally friendly by utilizing energy sources from nature such as wind energy, water, ocean waves, ocean currents, geothermal, and the sun.

In addition to utilizing various environmentally friendly energy sources, it is also necessary to pay attention to the ease of making the ECS form. The ease with which the ECS is manufactured depends on the nature and energy potential of the fluid flow to be utilized (working fluid). The properties and potential energy of fluid flow are quite large, namely the potential energy and kinetic energy of water.

The use of water flow energy to be converted into other forms of energy (one of which is a form of electrical energy) by ECS requires high ECS rigidity to be able to overcome the impact of

vibrations caused by the flow of water through the ECS body. One form of ECS with high rigidity is a screw turbine which is designed based on the Archimedes thread theory which is used to design pump impellers. Another advantage of the screw turbine is that it has a high L/d (L = turbine length and d = turbine diameter) so that it is suitable for use in narrow water flows (small rivers) [1] and low elevations (low head) [2]. known as micro-hydro flow energy.

The screw turbine is one of the reaction turbines that is used to take advantage of the potential energy of the water flow which changes the elevation of the water, namely the change in the potential energy of water into kinetic energy of water which is utilized by the blades (thread-shaped) to rotate the turbine. Utilization of water flow energy is possible because of the high density of water (998 kg/m^3) so that it is able to provide a compressive force (perpendicular to the screw surface) and a shear force (tangential to the screw surface) [3]. The resultant compressive force and shear force acting on the surface of the turbine thread will produce torque about the turbine axis.

The torque value of the screw turbine generated by the energy of the flow of water depends on the geometry (shape and size) of the thread and the width of the threaded end gap with the turbine casing as a place for water to flow. The results of the development of screw turbine geometry have been carried out by ECS experts including; Rorres (2000) obtained the optimum geometry of the screw turbine which was expressed in the ratio R1/R0 of the inner radius of the turbine (R1) with the outer radius of the threaded end (R0) namely [4], Nuembergk and Chris (2013) obtained the optimum gap between the tip of the thread and the turbine housing. [5], Tineke, at.al, (2015) obtained the pitch distance S using the triple thread type (N = 3) and the screw angle [6,7].

Studies in the form of numerical simulations on screw turbines have also been carried out by many numerical experts, including Reza Ali, et al. (2013) have performed numerical simulations using Simulink Matlab to predict the power that can be generated by screw turbines in low head water flows [8], Scott (2018) conducted screw turbine simulations using OpenFoam [9], Omar et.al. (2020) simulated a turbine with a single screw using Ansys

CFX-Fluent [10], Francesc (2019) and Edrisinghe, et.al., (2021) had simulated a screw turbine at an angle with variations in turbine rotation using Ansys CFX [11]. ,12], Alkistis and Vassilios (2021) performed a numerical simulation of CFD body dynamics with variations in the angle of inclination using 3D Flow [13]. The geometry and conditions of the screw turbine that have been carried out by [4,5,6,7,8,9,10,11,12,13] are summarized and shown in Table 1.

Ref	R_O	R_i	*Pitch*	*N*	*m*	β	α	h_O	c_O	Ket lain
[4]	-	-	-	-	-	-	-	-	-	R_i/R_O=0.54
[5]										
[6,7]	0.055	0.030	0.132	3	21	30	25, 35, 45	*(1/2)*R_O (2/3)R_O *(1)*R_O	0.3m/s 0.4m/s 0.5m/s	L=924 mm
[8]										
[9]	0.073025	0.037973	0.11684, 0.14605, 0.205232,	3	-	-	24.5	0.1125-0.1525m	0.5, 1, 2, 3, 4, 5, 7, liter/s	*L=0.5842m,* R_i/R_O=0.52, Solidwork, OpenFoam
[10]	0.065	0.035	0.015, 0.030, 0.070, 0.100, 0.120	1	12		30, 35, 40, 45		1.12-2.065 liter/s	*L=1m, Gap=2mm,* R_i/R_O=0.536, Solidwork, Ansys Fluent

[11]	0.950	0.508	1.907	3			22	1.05	0.87-5.20 m^3/s	*L=4.400m*, R_I/R_O=0.5347, Ansys CFX
[12]	1.2	0.643	0.836	3	-	-	45	5.2m	0.232 m^3/s	R_I/R_O=0.5358, Gap=5mm, rev=54.58 rpm, Solidwork, Ansys CFX
[13]	0.245	-	-	3	-	-	22, 25, 28, 32	1-5	0.15, 0.30, 0.45 m^3/s	L=2.55m, Solidwork, Flow-3D

Table 1.
Parameters of the screw turbine experimental model.

Based on the reference sources above, it is necessary to carry out a numerical simulation process of water flow with a free surface of multiphase flow model approach that passes through a screw turbine with the geometry and flow conditions according to the test results studied by [6,7]. The flow simulation model uses fluid flow interaction with a screw turbine which is treated as rigid body dynamics.

The free surface flow problem is very important to find a solution, because all hydroelectric power plants have a flow that can be modeled with free surface flow.

For the purpose of handling free surface flow problems, several computational fluid dynamics (CFD) techniques, called “mesh-grid” methods, including volume of fluid (VOF) [14], level-set [15], and constrained interpolation profile [16] have been proposed. Some studies have been conducted to simulate free surface flow around a moving screw turbine by using these methods.

Another solution for the free surface flow is the particle based CFD, called “mesh-free method” or “particle method.” Typical particle methods include Moving Particle Semi-implicit (MPS) [17]. Smoothed Particle Hydrodynamics (SPH), [18,19], and Particle Finite Element Method (PFEM) [20]. Particle methods have been successfully applied to the free surface flow problems. Koshizuka and Oka [17] proposed the original MPS method for simulating the incompressible fluid flow fragmentation. Imas et al [21]. simulated the flow around a surface-piercing body using the Smoothed Particle Hydrodynamics (SPH) method. Iida and Akimoto [22] employed mirror image particles to model a three-dimensional body surface in the MPS method. Colagrossi and

Landrini [23] presented a SPH method to simulate the two-dimensional interfacial flow. In their work, they suggested “ghost particles” for treating the smooth body boundary. Sueyoshi et al. [24] simulated the motion of floating body induced by water on the deck using the MPS method. Shibata et al. [25] developed a simulation method for shipping water based on the MPS method, and the numerical impact pressures on the deck were compared with the experimental results. Akimoto [26] simulated the fluid behavior induced by a planing body using the MPS method. The mirror image particles are also used to handle the body surface boundary. In these treatments, the mirror image particles near a sharp corner of body boundary showed excess or deficiency of particle density due to the singularity of shape. Dashtimanesh and Ghadimi [27] simulated the transom stern flow behind a rectangular planing hull by using their developed 3D-SPH code and compared with its experimental results. These research studies showed that the particle methods had advantages of capturing free surface from highly deformed flow. Due to ease in capturing nonlinear free surface, the particle methods have been

successfully applied to a great diversity of problems arising in many engineering fields.

This paper aims at analyzing the flow around a screw turbine using the MPS method, which is one of the widely used particle methods. This paper addresses the modified MPS method with some modifications, such as Laplacian compensation model in the region near the body boundary, collision model between fluid particles and wall particles, several treatment techniques for the opened boundary, and full-domain simulation technique.

BAB 2
EXPERIMEN MODEL

Experimental Model

Test Bed Installation

The physical model of the screw turbine includes the geometry (shape and size) of the screw turbine which is described in Table 1 as well as the schematic model of the test in Figure 1, all of which are based on research results [6,7].

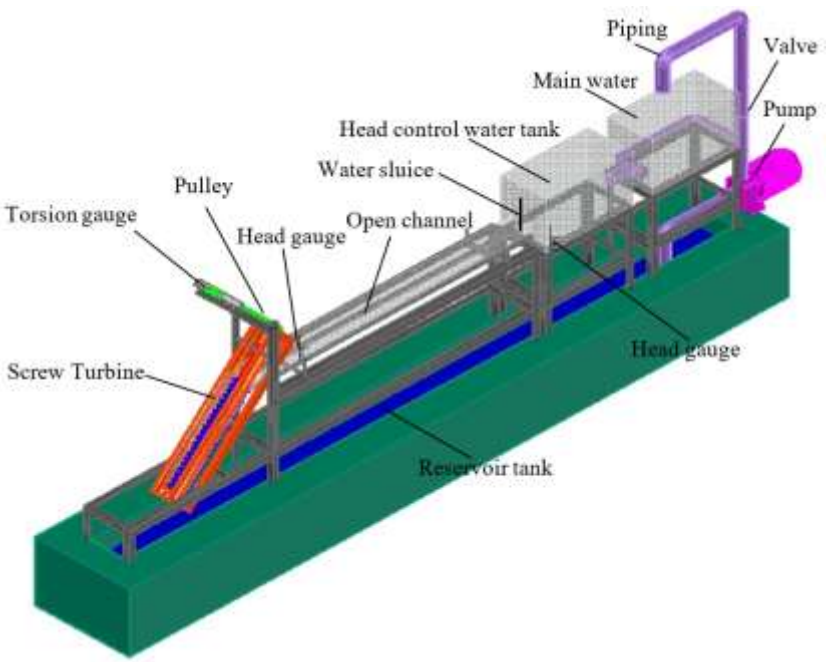

Figure 1. The screw turbine test bed installation [6,7].

Experimental Procedure

The threaded material is made of flexyglass with a pipe size for the shaft of 60 mm, blade height of 25 mm, range of 2.4Ro, radius ratio (R_1/R_o) is 0.54, the number of turns of thread is 21, and the thread angle is 30^0. The screw turbine model is shown in Figure 1. The method of data collection is firstly the installation settings according to the specified parameters and the measuring instrument is calibrated. Test running the water flow from the reservoir tank is flowed through a pump (pump) with specifications Hmax 22 m, power 0.75 kW, rotation n 2850 rpm, Qmax 600 L/min, to the holding tank (main water) with discharge settings through the valve (Valve) and the flow rate is regulated through the elevation of the head control water tank and elevation control with a head gauge at the exit of the tank (Water sluice). Next, the water flows into a rectangular channel (Open channel) with a length of 210 cm and a width of 12 cm, which is set to the depth of the turbine inlet as the characteristic length y with a head gauge. The water flow then enters the screw turbine and is then accommodated in the reservoir tank and the flow is returned to the main water tank through the pump continuously.

After that, start the data collection process by adjusting the tilt position of the turbine shaft , adjusting the characteristic length variable y by controlling the water sluice out of the tank and the water depth in the tank (Head control water tank) until the condition is steady. Measurement data taken are turbine rotation using a tachometer, flow visualization using a digital camera, and rotational braking load (torque) using a spring balance (Torsion gauge) connected via pulleys and belts (pulleys). Measurement data were taken respectively at variations in flow velocity (co) 0.3 m/s, 0.4 m/s, 0.5 m/s at each variation of the shaft slope (α) 25°, 35°, 45°. The measurement data was repeated three times for each variable [6,7].

The screw turbine model has a specific dimension. The turbine screw is a three bladed type screw made from flexi-glass and has a 60 mm diameter shaft, a 25 mm blade height with a 2.4 Ro blade screw pitch, a radius ratio (R_1/R_o) of 0.54 and a screw angle of 30°. Before the data collection, all measuring devices had been calibrated. The water flow test running was firstly proceeded by pumping water from the water reservoir tank goes into the main

water tank. The flow rate was set through a head controller in the in the sedative tank at the exit of the tank. Secondly, the water flow into the rectangular open channel was arranged into a certain turbine head inflow (ho). This rectangular open channel is the guide for the water inflow going inside the turbine, passing through the turbine blades, pushing the turbine blade to rotate and finally producing the turbine torque. The water output from the turbine was then catch back to the reservoir and ready to be pump back to the water reservoir tank. The next step is preparing for the data collection where the data variation is adjusting the turbine axis angle (α), setting the turbine head inflow by adjusting the small water gate on the water tank bottom to get a steady state water flow. The data taken are the turbine rotation using a tachometer, the water flow visualization using a camera and turbine torque using a small prony brake. All the data was taken at a head ho variation of 1Ro, 2/3Ro and 1/2Ro respectively under a flow rate variation of 0.3 m/s, 0.4 m/s, 0.5 m/s at a turbine axis angle α of 25°, 35°, 45° respectively. The data measurement was repeated three times for each variable [6,7].

Principals of Characteristics of Turbines

The water power available due to the difference of the head and can be mechanically extracted using the power adapter which is the turbine. The mechanical power generated by the turbine can be converted to electrical power by electrical generators. The characteristics of the Archimedes screw turbine (figure 2) will be estimated depending on the following analysis on reference [11,28].

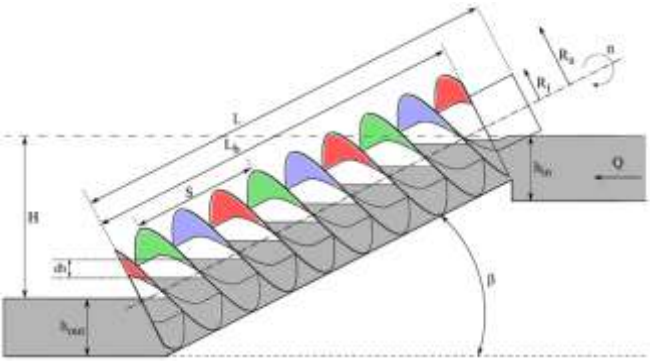

Figure 2. Geometrical parameters of the screw turbine [11].

Based on Figure 1, if P_{hyd} is represent the power supplied by the water, ρ is water density, $\vec{g}$ is gravitation acceleration, Q is the flow rate and H is the head from top to end of the blade, then the

hydraulic power that be supplied by the water is given below [11,28]:

$$P_{hyd} = \rho \vec{g} Q H \quad (1)$$

If torque of the screw turbine is $\vec{T}$ and angular velocity is $\vec{\omega}$ then the mechanical power produced by the screw turbine (P_{mec}) and is estimated below [11,28]:

$$P_{mec} = \vec{T} \cdot \vec{\omega} \quad (2)$$

The efficiency of the screw turbine is calculated by [11,28]

$$\eta = \frac{P_{mec}}{P_{hyd}} \times 100\% \quad (3)$$

BAB 3
NUMERICAL MODEL

Particlework CFD Code

Simulation process is using Particlework Computational Fluid Dynamics (CFD) code. Particleworks is a Moving Particle Simulation (MPS) based CFD software package. Using a novel calculation technique that does not require grid generation, it is capable of simulating the fluid dynamics associated with free surface or splashing, etc. in a precise and stable manner by representing fluid as a collection of particles. It discretizes the Navier-Stokes equations using the gradient model and the Laplacian model and computes the results. Even when the surface of a fluid changes drastically or a liquid coalesces or separates, there is no need for processing using, for example, conventional grid-based techniques, and predefinition of a grid in the region in which fluid may splash is also unnecessary. Particleworks is coming into use in a wide range of industrial fields thanks to its ability to handle problems that are difficult to analyze using conventional CFD software [29].

Governing Equations

The MPS Method was first published by Koshizuka and Oka (1996) [17] and has been used in research in various areas of engineering and science since then. The MPS Method uses the interaction model of particles that corresponds to the differential operator, and the governing equations are discretized by the interaction model. In the discretization, the weight function is applied. The variable of the weight function is the distance between the particles. Since the particles move by retaining such variables as velocity and pressure, they do not require a grid as in the numerical methods of the finite difference method and finite element method etc.

The MPS method is an analytical method dealing with incompressible flow, in which continuum mechanics is discretized using particles. The fundamental governing equations of the MPS method are a continuum equation and Navier-Stokes equations expressed as follows.

$$\frac{D\rho}{Dt} = 0 \tag{4}$$

$$\frac{D\vec{u}}{Dt} = -\frac{\nabla p}{\rho} + \nu\nabla^2\vec{u} + \vec{f} \quad (5)$$

Where $\frac{D}{Dt}$ expresses a Lagrangian derivation. ρ is density, $\vec{u}$ velocity, p pressure, ν kinematic viscosity coefficient, and $\vec{f}$ body force.

Particle Interaction Model

Interaction between two particles is calculated only for those particles that have moved closer than a fixed value given to the distance between two particles. Figure 3 shows the distance over which an interaction has an effect is designated as the "effective radius r_e" and the influential domain around a particle i. The particle i only interacts with blue-colored particles in the influential domain [30]

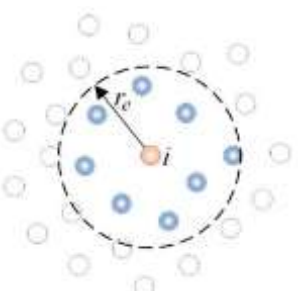

Figure 3. effective radius r_e [30].

In the MPS, it is considered that particles interact with each other based on the following weight function [30]

$$w\left(\left|\vec{r}_{ij}\right|\right)=\begin{cases}\dfrac{r_e}{\left|\vec{r}_{ij}\right|}-1 & \rightarrow \quad \left(\left|\vec{r}_{ij}\right|<r_e\right) \\ 0 & \rightarrow \quad \left(\left|\vec{r}_{ij}\right|\geq r_e\right)\end{cases} \tag{6}$$

where subscripts i and j express particle numbers, in addition, $\vec{r}_{ij}=\vec{r}_j-\vec{r}_i$, where $\vec{r}_i$ is the position vector of particle i. As can be seen in equation (6), the weight of interaction between two particles is related to the distance between them. When the distance gets nearer, the weight of interaction gets larger. If the distance between two particles is larger than r_e, their interaction is neglected. Figure 4 show the curve of weight function.

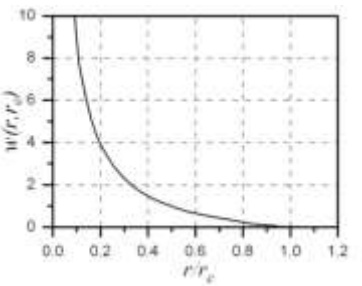

Figure 4. weight function.

Particle number density is a dimensionless quantity expressing the density of particle placement, and is a parameter unique to the MPS method. The particle number density is defined by

$$n_i = \sum_{j \neq i} w\left(\left|\vec{r}_{ij}\right|\right) \tag{7}$$

In particle placement that satisfies incompressible conditions, the particle number density is a fixed value (particle number density at the initial state n_0). For the particle number density at the initial state n_0, the particle number density in the state shown in the Figure 5 is used, where particles are arranged in an orthogonal grid and separated by the initial particle distance.

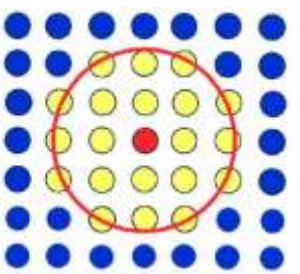

Figure 5. Particle Number Density [29].

Modeling Term

The gradient vector of a scalar quantity between two points i and j can be approximated by the product of the variation of a physical quantity ϕ divided the distance times the unit direction. In MPS, the gradient vector is modelled using the weight function to obtain a gradient vector of the particle i as [29,31],

$$\langle \nabla \phi \rangle_i = \frac{d}{n^0} \sum_{j \neq i} \frac{\left(\phi_j - \phi_i\right) \vec{r}_{ij}}{\left|\vec{r}_{ij}\right|^2} w\left(\left|\vec{r}_{ij}\right|\right) \tag{8}$$

The gradient model is used for calculating velocity correction by pressure.

where d is the number of space dimension and ϕ_i is taken as the minimum value of ϕ_j within the interaction ratio, this is good for numerical stability as forces between particles are always repulsive as $\phi_j - \phi_i$ is positive.

The Laplacian operator is modelled using a transient diffusion equation, where part of the quantity ϕ in particle i is distributed to its neighbour's particles j using the weight function. The Laplacian model is used for calculating viscosity and pressure. In

the MPS method, the Laplacian model given the following discretisation [29,31],

$$\left\langle \nabla^2 \phi \right\rangle_i = \frac{2d}{\lambda n^0} \sum_{j \neq i} \left(\phi_j - \phi_i \right) w\left(\left| \vec{r}_{ij} \right| \right) \tag{9}$$

$$\lambda = \frac{\sum_{j \neq i} \left| \vec{r}_{ij} \right|^2 w\left(\left| \vec{r}_{ij} \right| \right)}{\sum_{j \neq i} w\left(\left| \vec{r}_{ij} \right| \right)} \tag{10}$$

with λ is a parameter to ensure that the variance increase is equal to the analytical solution.

The gradient model is used for the formulation of the symmetric gradient model and calculating the source term of the pressure Poisson equation using divergence of velocity. The divergence model is discretized to [29]

$$\left\langle \nabla \vec{u} \right\rangle_i = \frac{2d}{n^0} \sum_{j \neq i} \frac{\left(\vec{u}_j - \vec{u}_i \right) \vec{r}_{ij}}{\left| \vec{r}_{ij} \right|^2} w\left(\left| \vec{r}_{ij} \right| \right) \tag{11}$$

Algorithm

In the MPS method, the Navier-Stokes equations are divided into two stages, and all terms are solved explicitly, except for the pressure term, which is solved implicitly [29,31].

Explicit calculations of terms except the pressure term

$$\frac{\vec{u}^{*}-\vec{u}^{k}}{\Delta t}=\nu\nabla^{2}\vec{u}^{k}+\vec{g} \tag{12}$$

Implicit calculation of pressure

$$\nabla^{2}p^{k+1}=\frac{\rho}{\Delta t^{2}}\frac{n^{*}-n^{0}}{n^{0}} \tag{13}$$

Velocity and position correction by the pressure gradient

$$\frac{\vec{u}^{k+1}-\vec{u}^{*}}{\Delta t}=-\frac{\nabla p^{k+1}}{\rho} \tag{14}$$

where n is the particle number density, and n^{0} is the particle number density at the initial state, both of which are explained later Superscript k expresses the time step Superscript * expresses a physical quantity at the stage where the explicit calculation has been completed. The diagram below shows the calculation algorithm of the MPS method.

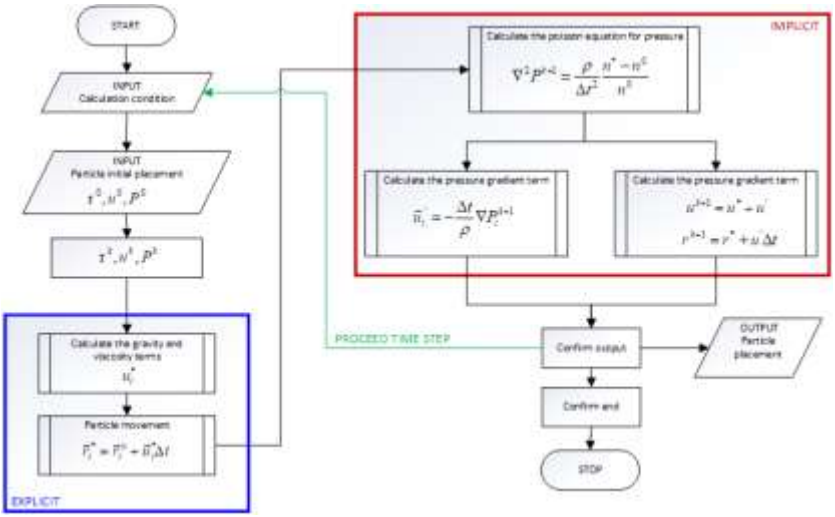

Figure 6. calculation algorithm of the MPS method [29].

Free Surface Condition

In the MPS method, as a Dirichlet boundary condition for pressure calculation, pressure zero is given to particles on free surface. A particle whose particle number density satisfies the following condition is considered to be on the free surface [29].

$$n_i < \beta n^0 \tag{15}$$

with β is a density threshold, and the default value in Particleworks is 0.97.

Gravity

The effect of gravity is considered by time integration as follows [29].

$$\vec{u}_i^* = \vec{u}_i^k + g\Delta t \tag{16}$$

Viscosity

The effect of viscosity is calculated using the Laplacian model, and is time-integrated as shown below [29].

$$\vec{u}_i^* = \vec{u}_i^k + \frac{2d}{\lambda n^0}\Delta t \sum_{j \neq i} v_{ij}\left(\vec{u}_j^k - \vec{u}_i^k\right) w\left(\left|\vec{r}_{ij}^k\right|\right) \tag{17}$$

The kinematic viscosity coefficient v_{ij} between particles is defined as follows:

- Between the same type of fluids: The harmonic average of the kinematic viscosity coefficients of individualparticles is used.
- Between different types of fluid: The result obtained by multiplying the harmonic average of the kinematic viscosity coefficients of individual particles by the parameter input in the Fluid Combination box when setting the kinematic viscosity coefficient.

- Between the fluid and particle wall, rigid body, powder, or polygon wall: The result obtained by multiplying the kinematic viscosity coefficient of an individual particle by the parameter input in the Slip Conditions box.

Rigid Body

Particleworks, in the same manner as fluids, expresses and analyzes rigid bodies as a set of particles with mass. The mass of a rigid body M is derived from the equation (20) using the mass m_i of an individual particle i.

$$M = \sum_i m_i \tag{20}$$

The center of mass of a rigid body $\vec{x}$ is derived from the equation (21), using the mass of the rigid body M, the position $\vec{r}$ of a particle i in the rigid body, and the mass of particle m_i.

$$\vec{x} = \frac{\sum_i m_i \vec{r}_i}{M} \tag{21}$$

Temporal change of the center of mass of a rigid body $\frac{d\vec{x}}{dt}$ and the translational velocity of the rigid body $\vec{v}$ have the relation defined by the equation (22).

$$\frac{d\vec{x}}{dt} = \vec{v} \tag{22}$$

The translational velocity of a rigid body $\vec{v}$ and the momentum of the rigid body $\vec{P}$ are derived from the equations (23) using the mass of the whole rigid body M .

$$\vec{P} = M\vec{v} \rightarrow \vec{v} = \frac{\vec{P}}{M} \tag{23}$$

The angular velocity of a rigid body $\vec{\omega}$ and the angular momentum of the rigid body $\vec{L}$ have the relation defined by the equation (24).

$$\vec{L} = I_{ab}\vec{\omega} \rightarrow \vec{\omega} = I_{ab}^{-1}\vec{L} \tag{24}$$

However, I_{ab} is the inertia tensor of the rigid body.

Particleworks finds $\frac{d\vec{L}}{dt}$ using the equation (25), which differentiated the equation (24), and the equation (33), and then,

$$\frac{d\vec{\omega}}{dt} = I_{ab}^{-1}\frac{d\vec{L}}{dt} \tag{25}$$

The inertia tensor of a rigid body $I(t)ab$ at time t is expressed as given below, using the mass mi of individual particle i in the rigid body at time t, and the relative position with respect to the gravity center of the rigid body $\vec{r}_{it} = \left(\vec{r}_{ixt} + \vec{r}_{iyt} + \vec{r}_{izt}\right)$

$$I(t)_{ab} = \sum_i m_i \begin{pmatrix} r_{iyt}^2 + r_{izt}^2 & -r_{ixt}r_{iyt} & -r_{ixt}r_{izt} \\ -r_{ixt}r_{iyt} & r_{ixt}^2 + r_{izt}^2 & -r_{iyt}r_{izt} \\ -r_{ixt}r_{izt} & -r_{iyt}r_{izt} & r_{ixt}^2 + r_{iyt}^2 \end{pmatrix} \tag{26}$$

If the inertia tensor is calculated using the equation (26) for each step, this requires high calculation costs; therefore, it is derived from the equation (27) using the rotation matrix of the rigid body $R(t)_{ab}$ at time t.

$$I(t)_{ab} = R(t)_{ab}\, I_{init} R(t)_{ab}^{T} \tag{27}$$

However, I_{init} is the inertia tensor at the initial state, and is expressed as shown below using the mass mi of each particle i in the rigid body in the initial state, and the relative position with respect to the gravity center of the rigid body $\vec{r}_{i0} = \left(\vec{r}_{ix0} + \vec{r}_{iy0} + \vec{r}_{iz0}\right)$

.

$$\vec{I}_{init} = \sum_i \left\{ \begin{array}{l} m_i \begin{pmatrix} r_{iyt}^2 + r_{izt}^2 & -r_{ixt} r_{iyt} & -r_{ixt} r_{izt} \\ -r_{ixt} r_{iyt} & r_{ixt}^2 + r_{izt}^2 & -r_{iyt} r_{izt} \\ -r_{ixt} r_{izt} & -r_{iyt} r_{izt} & r_{ixt}^2 + r_{iyt}^2 \end{pmatrix} + \\ \frac{2}{3} \rho (2L)^3 L^2 \begin{pmatrix} 1 & 0 & 0 \\ 0 & 1 & 0 \\ 0 & 0 & 1 \end{pmatrix} \end{array} \right\} \quad (28)$$

(The second term on the right-hand side is the inertia tensor of a cube of side $2L$. A particle is treated as a cube of side $2L$, not a material point; therefore, this term is needed)

The velocity $\vec{u}_i$ of a particle i making up a rigid body is derived from the equation (29) using the translational velocity of the rigid body $\vec{v}$, the angular velocity $\vec{\omega}$, and the relative position vector $\vec{r}_{it}$ of particle i with respect to the gravity center of the rigid body.

$$\vec{u}_i = \vec{v} + \vec{\omega} \times \vec{r}_{it} \quad (29)$$

A torque added to a rigid body $\vec{T}$ is derived from the equation (4.14) using an external force added to the rigid body $\vec{F}$, and the relative position vector $\vec{r}_f$ of the point of application of the external force with respect to the gravity center of the rigid body.

$$\vec{T} = \vec{r}_f \times \vec{F} \quad (30)$$

When an external force is added, the change of a rigid body's momentum $\frac{d\vec{P}}{dt}$, and the change of the rigid body's angular momentum $\frac{d\vec{L}}{dt}$ are derived from the equations (31) and (32) using the external force added to the rigid

body $\vec{F}$, and the torque added to the rigid body $\vec{T}$.

$$\frac{d\vec{P}}{dt} = \vec{F} \tag{31}$$

$$\frac{d\vec{L}}{dt} = \vec{T} \tag{32}$$

To express the attitude of a rigid body (rotation state), a rotation matrix is used. Rotation matrix R_{ab} is a 3 by 3 matrix as defined by the equation (33).

$$R_{ab} = \begin{pmatrix} r_{xx} & r_{xy} & r_{xz} \\ r_{yx} & r_{yy} & r_{yz} \\ r_{zx} & r_{zy} & r_{zz} \end{pmatrix} \tag{33}$$

The rotation matrix of the initial state rigid body R_{ab}^{0} is set by

$$R_{ab}^{0} = \begin{pmatrix} 1 & 0 & 0 \\ 0 & 1 & 0 \\ 0 & 0 & 1 \end{pmatrix} \tag{34}$$

When the rotation matrix of the rigid body at a certain time is R_{ab} , and when considering a particle whose relative vector with respect to the gravity center of the rigid body at the initial state is $\vec{p}_0$, the particle's relative position vector $\vec{p}$ with respect to the gravity center of the rigid body at the current time is derived from the equation (35)

$$\vec{p} = R_{ab}\vec{p}_0 \tag{35}$$

To deal with rotation information of rigid bodies, Particleworks uses quaternion, which has a smaller volume of data compared to a rotation matrix and is efficient. Quaternion $\vec{q} = \left[s, v_x, v_y, v_z \right]$ and rotation matrix R_{ab} have the following relation.

$$R_{ab} = \begin{pmatrix} 1-2v_y^2-2v_z^2 & 2v_xv_y-2sv_z & 2v_xv_z+2sv_y \\ 2v_xv_y+2sv_z & 1-2v_x^2-2v_z^2 & 2v_yv_z+2sv_x \\ 2v_xv_z-2sv_y & 2v_yv_z+2sv_x & 1-2v_x^2-2v_y^2 \end{pmatrix} \tag{36}$$

Quaternion $\vec{q}(t)$ is updated to $\vec{q}(t+dt)$, using the equations (37) and (38) given below, the rotation axis of the rigid body $\vec{a}$ and the rotation angle θ.

$$d\vec{q} = \left[\cos\frac{\theta}{2}, \vec{a}\sin\frac{\theta}{2} \right] \tag{37}$$

$$\vec{q}\left(t + dt\right) = \vec{q}\vec{d}q \tag{38}$$

The rotation axis $\vec{a}$ and the rotation angle θ are derived from the equation (39) and (40) below, using the angular velocity $\vec{\omega}$ and time step.

$$\vec{a} = \frac{\vec{\omega}}{|\vec{\omega}|} \tag{39}$$

$$\theta = |\vec{\omega}|\Delta t \tag{40}$$

Collision and Friction of Particles

To deal with particle crash response, Particleworks employs the penalty method, which allows for the caving in of particle surfaces, and adds a repulsive force in accordance with the amount of caving in.

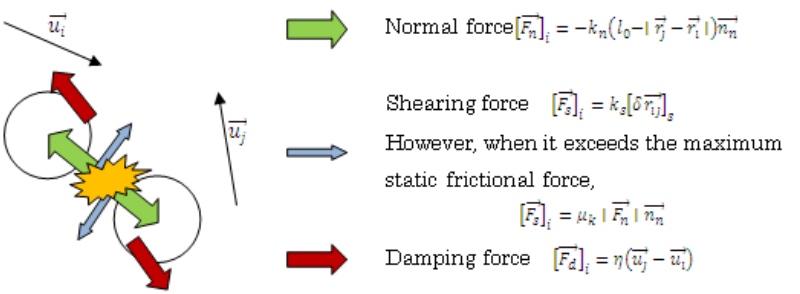

Figure 7. schematic drawing of interactivity occurring by collision [29].

For the particles detected as having collided, three types of interactivity $\vec{F}$, normal force $\vec{F}_n$, shearing force $\vec{F}_s$, and damping force $\vec{F}_d$ are given to them as defined by the equation (41) .

$$\vec{F} = \vec{F}_n + \vec{F}_s + \vec{F}_d \tag{41}$$

Let the particles detected as having collided be particle i and particle j respectively, then, the normal force $\vec{F}_n$ that affects particle i and particle j is derived from the equation (42), using the positions $\vec{r}_i$ and $\vec{r}_j$ of particles i and j, the normal spring constant k_n, and the particle diameter l_0.

$$\left|\vec{F}_n\right|_i = -k_n\left(l_0 - \left|\vec{r}_j - \vec{r}_i\right|\right)\vec{n}_n \rightarrow \left|\vec{F}_n\right|_j = -\left|\vec{F}_n\right|_i \tag{42}$$

The relative position $\vec{r}_{ij}^{\,0} = \vec{r}_j^{\,0} - \vec{r}_i^{\,0}$ of particle j with respect to particle i at the time when the collision of particle i and particle j was detected for the first time, is retained, and the displacement $\delta\vec{r}_{ij}$ of the relative position is derived from the equation (43),

using the relative position $\vec{r}_{ij} = \vec{r}_j - \vec{r}_i$ of particle j with respect to particle i at the current time.

$$\delta\vec{r}_{ij} = \vec{r}_j - \vec{r}_i^{\,0} \tag{43}$$

For the normal component of the displacement of the relative position (direction component perpendicular to the straight line connecting the centers of particle ij), the normal unit vector

$$\vec{n}_n = \frac{\vec{r}_{ij}}{\left|\vec{r}_{ij}\right|} \tag{44}$$

is used, and

$$\left[\delta\vec{r}_{ij}\right]_n = \left(\delta\vec{r}_{ij} \cdot \vec{n}_n\right)\vec{n}_n \tag{45}$$

is given; therefore, the shearing component of the displacement of the relative position of particle j with respect to particle i is given by

$$\left[\delta\vec{r}_{ij}\right]_s = \delta\vec{r}_{ij} - \left[\delta\vec{r}_{ij}\right]_n \tag{46}$$

Using this $\left[\delta\vec{r}_{ij}\right]_s$ and the shearing spring constant k_s, the shearing force (friction force) $\vec{F}_s$ added to particles due to collision is derived from the equation (48).

$$\left[\vec{F}_s\right]_i = k_s\left[\delta\vec{r}_{ij}\right]_s \rightarrow \left|\vec{F}_s\right|_i = -\left|\vec{F}_s\right|_j \tag{47}$$

The shearing force $\vec{F}_s$ is controlled and will not exceed the maximum static frictional force. More specifically, let the static friction coefficient between particles be μ_s, and the normal force be $\vec{F}_n$, and then, the maximum static frictional force $\left[\vec{F}_s\right]_{\max}$ is expressed by

$$\left[\vec{F}_s\right]_{\max} = \mu_s\left|\vec{F}_n\right| \tag{48}$$

Therefore, when the shearing force is the maximum static frictional force or below (when $\left|\vec{F}_s\right| \le \left|\left[\vec{F}_s\right]_{\max}\right|$), $\vec{F}_s$ is used as the shearing force. However, when the shearing force exceeds the maximum static frictional force (when $\left|\vec{F}_s\right| > \left|\left[\vec{F}_s\right]_{\max}\right|$), letting the kinetic friction coefficient between particles be μ_k, the kinetic friction force shown in the equation (49) is used as the shearing force $\vec{F}_s$

$$\left|\vec{F}_s\right|_i = \mu_k\left|\vec{F}_n\right|\vec{n}_n \rightarrow \left|\vec{F}_s\right|_j = -\left|\vec{F}_s\right|_i \tag{49}$$

When the velocity of particle i and particle j, which were detected as having collided, are assumed to be $\vec{u}_i$ and $\vec{u}_j$ respectively, the damping force $\vec{F}_d$ that affects particle i and particle j is derived from the equation (50) using a damping coefficient η

$$\left|\vec{F}_d\right|_i = \eta\left(\vec{u}_j - \vec{u}_i\right) \rightarrow \left|\vec{F}_d\right|_j = -\left|\vec{F}_d\right|_i \tag{50}$$

The above-mentioned spring constant k and damping coefficient η are derived from the equations (51) and (52) using an initial time increment t_{init} and a reduced mass m_{ij}.

$$k = \tilde{k}\frac{m_{ij}}{\Delta t_{init}^2} \tag{51}$$

$$\eta = \tilde{\eta}\frac{m_{ij}}{\Delta t_{init}} \tag{52}$$

However, $\tilde{k}$ is a value known as a spring constant ratio, and $\tilde{\eta}$ is a value termed a damping coefficient ratio, and these values satisfy $0 \leq \tilde{k} \leq 1$, $0 \leq \tilde{\eta} \leq 1$. Moreover, the reduced mass m_{ij} is derived from the equation (53) using the mass m_i and mass m_j

of particle i and particle j, which were detected as having collided.

$$m_{ij} = \frac{m_i m_j}{m_i + m_j} \tag{53}$$

Behavior of a rigid body is calculated in the following manner:

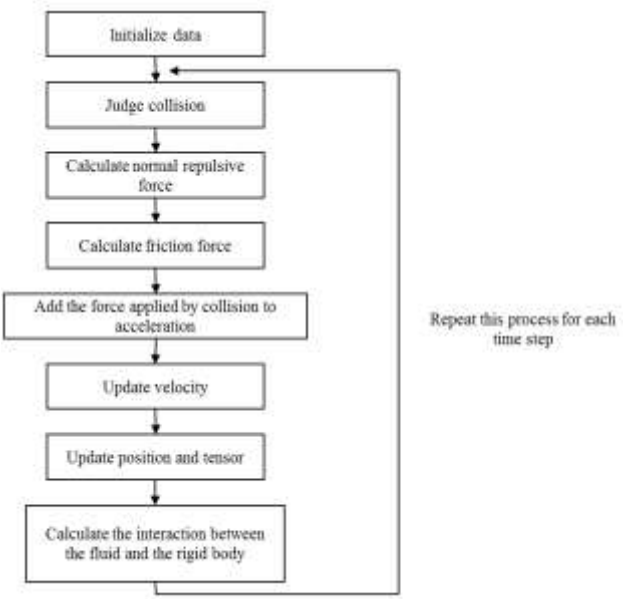

Figure 8. flow chart of rigid body is calculated.

Screw Turbine Geometry

The design of the Screw Turbine was made by Solidworks CAD Code with same the dimensions of experimental work with

change some parameters for study number of cases. Figure 9 shows the screw turbine that constructed using solid works.

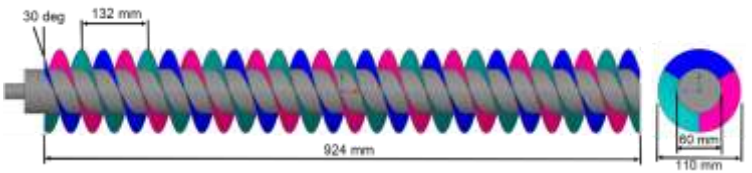

Figure 9. Screw turbine geometry.

The screw turbine is placed in an open water channel container with an inclination angle of 25o, 35o and 45o as shown in the figure below.

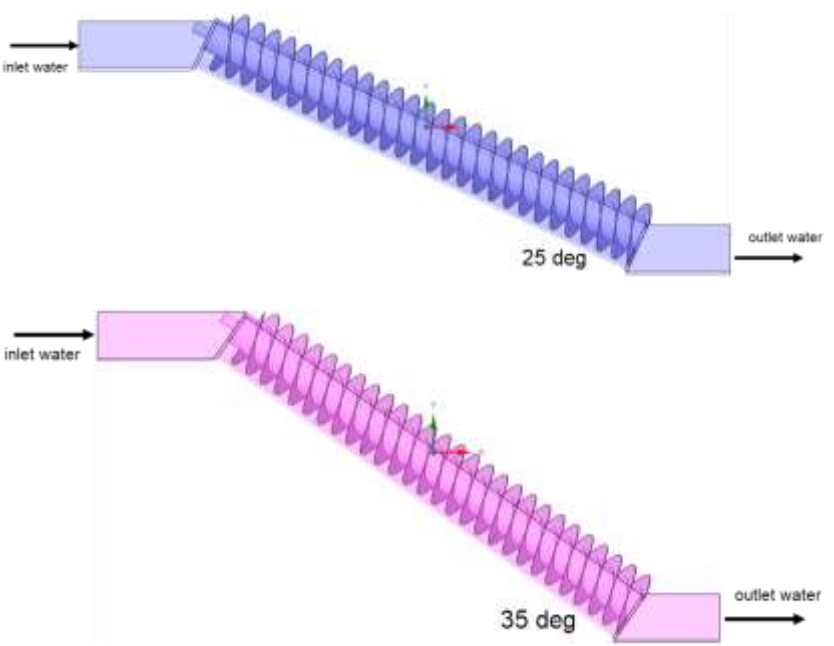

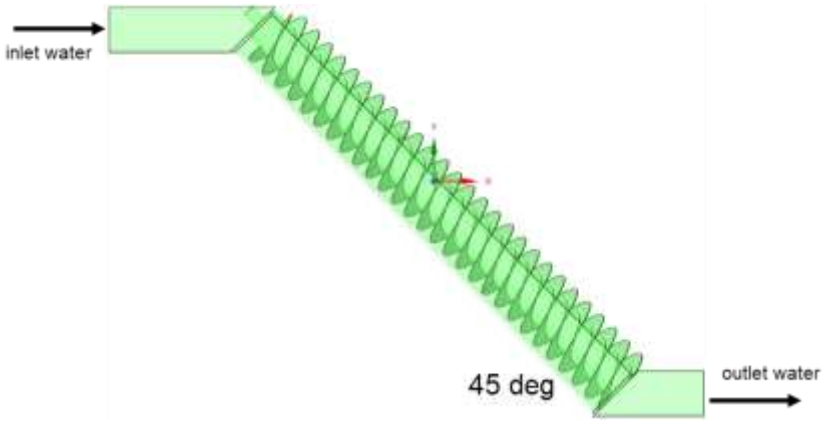

Figure 10. Type Screw turbines geometry and open channal with slope 25º, 35º and 45º.

Tabel 2. Parameters for solid and fluid domains.

Fluid type	Properties	Value	Unit	Description
Water liquid	Density	988.7	kg/m^3	-
	Kinematic viscosity	$1x10^{-6}$	m^2/s	-
	Surface tension coefficient	0.072	N/m	-
	Contact angle	90	deg	-
Screw turbine (flexyglass)	Density	1190	kg/m^3	-
	Restitution Coefficient	0.5	-	-
	Static friction coefficient	0.1	-	-

	Dynamic friction coefficient	0.1	-	-
	massa	2.6	kg	-
Inertia moment tensor	I_{xx}	0.0013	$kg.m^2$	Inertia moment of mass to turbine axis
	I_{yy}	0.155	$kg.m^2$	Inertia moment of mass to normal turbine axis
	I_{zz}	0.155	$kg.m^2$	Inertia moment of mass to normal turbine axis
	adiabatic	-	-	-
Turbulent Model	Large-Eddy Simulation model	-	-	-

BAB 4
CALCULATION ALGORITHM

The mass flow rate calculated using the MPS method in transient conditions for 20 seconds is as shown in Figure 11.

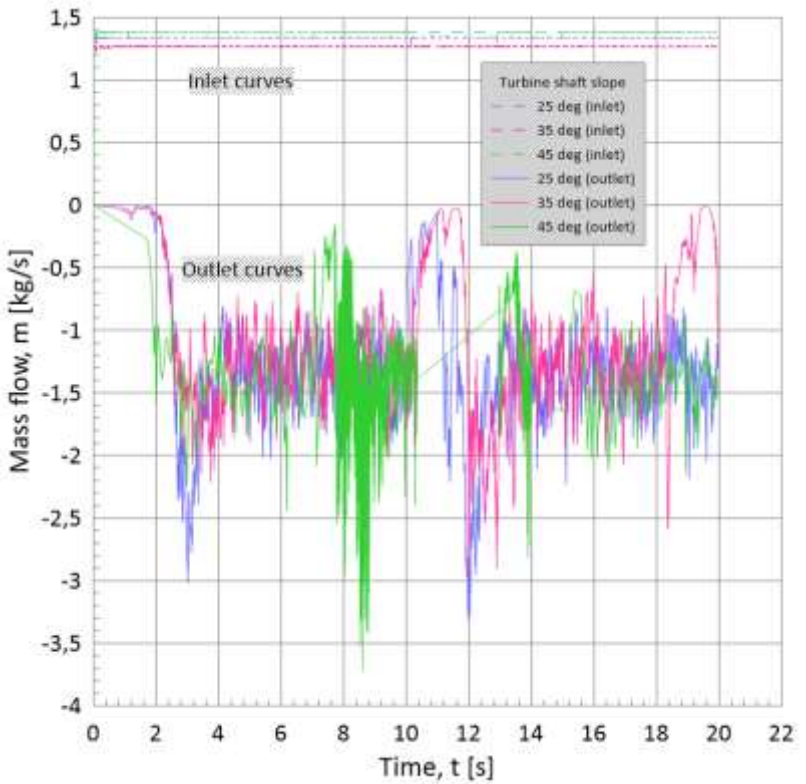

Figure 11. Curves transient of mass flow with slope 25º, 35º and 45º.

As seen in Figure 11, the average value of the mass flow out (outlet curve) which is negative has a tendency to be the same

value as the mass flow in (inlet curves). This shows that the flow tends to be steady at t = 4 seconds and fluctuates at t = 10-12 seconds due to the accumulation of water or water spills in the middle of the screw turbine, thereby reducing the mass flow out. The mass of water flowing along the surface of the turbine thread will produce a hydraulic force with a force component in the form of shear force, as in Figure 12. The shear force vector component has a certain position relative to the turbine shaft axis, so it will cause the turbine to rotate. The turbine rotational speed value is derived based on equation (54).

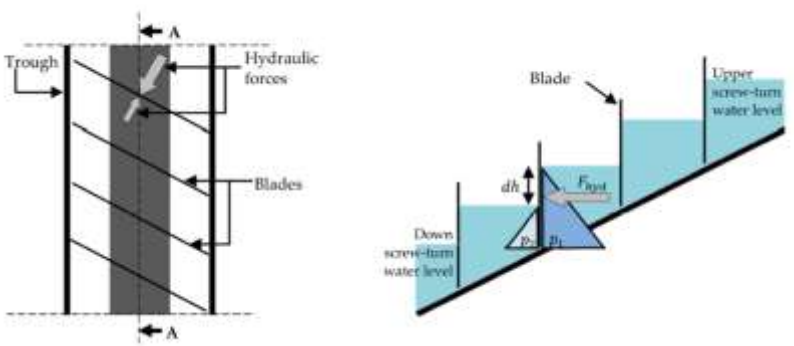

Figure 12. Forces acting on idealized Archimedean screw blade. (left) plan view (right) side view of cross-section on plane A-A [12].

Equation solution of an angular speed of screw turbine on every time step is written by

$$\vec{\omega}^{k+1} = \vec{\omega}^{k} + \frac{d\vec{\omega}}{dt}\Delta t \tag{54}$$

The Figure below shows the angular speed curves calculation algorithm of the MPS method for screw turbine 25º, 35º and 45º.

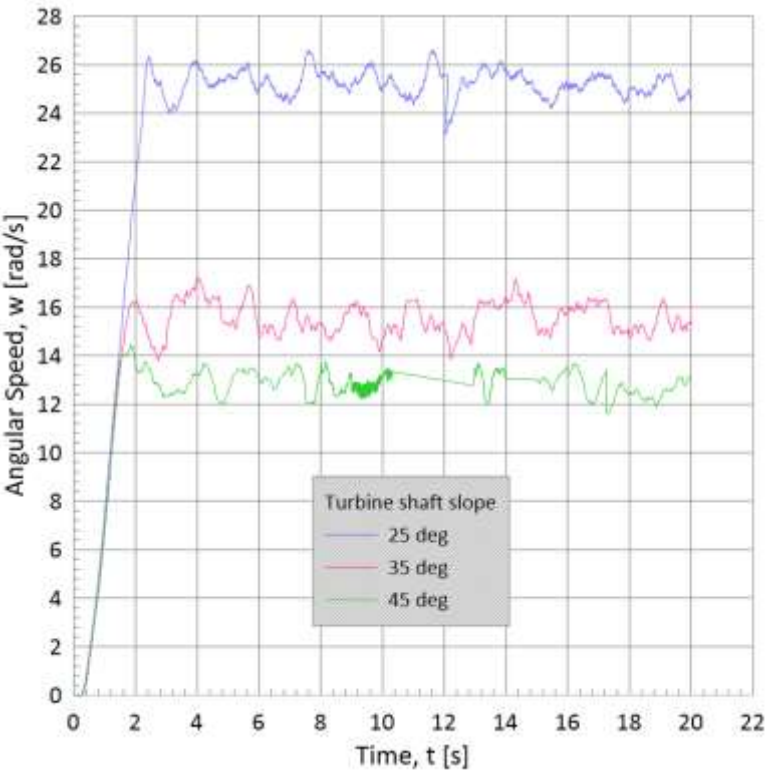

Figure 13. Curves transient of angular speed with slope 25º, 35º and 45º.

A torque added to a rigid body $\vec{T}$ is derived from the equation (55) using an external force added to the rigid body $\vec{F}$, and the

relative position vector $\vec{r}_f$ of the point of application of the external force with respect to the gravity center of the rigid body.

$$\vec{T} = \vec{r}_f \times \vec{F} \tag{55}$$

When an external force is added, the change of a rigid body's momentum $\frac{d\vec{P}}{dt}$, and the change of the rigid body's angular momentum $\frac{d\vec{L}}{dt}$ are derived from the equations (56) and (57) using the external force added to the rigid body $\vec{F}$, and the torque added to the rigid body $\vec{T}$.

$$\frac{d\vec{P}}{dt} = \vec{F} \tag{56}$$

$$\frac{d\vec{L}}{dt} = \vec{T} \tag{57}$$

The Figure 14 shows the torque curves calculation algorithm of the MPS method for screw turbine 25^o, 35^o and 45^o.

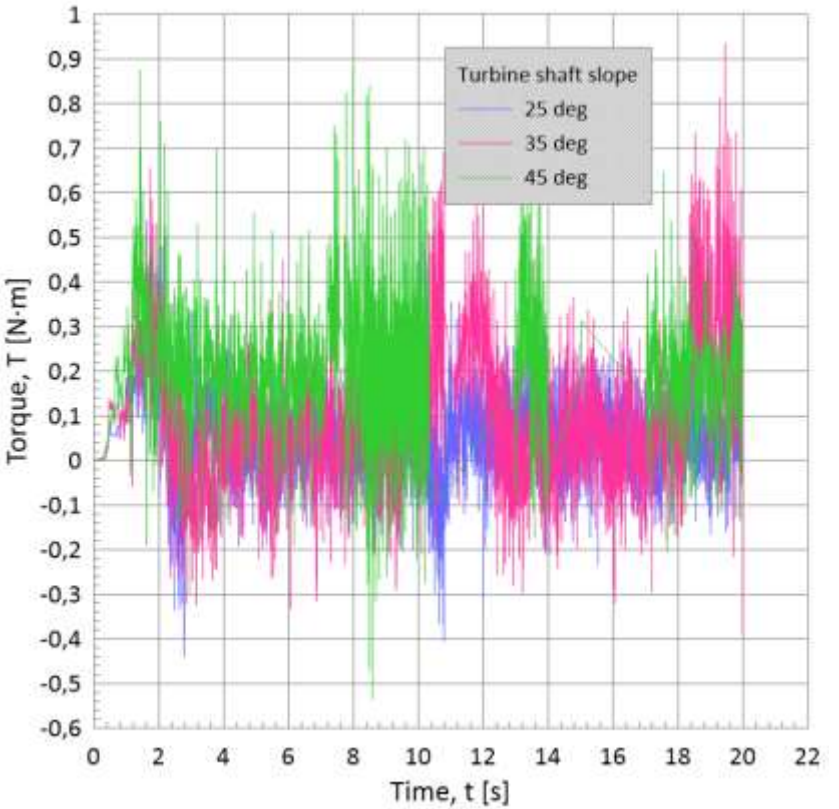

Figure 14. Curves transient of torque with slope 25º, 35º and 45º.

The results of calculations using equation (2) or the result of multiplying the values of the angular speed curve (figure 12) and torque curve (figure 13) become mechanical power in transient conditions for 20 seconds as shown in Figure 15.

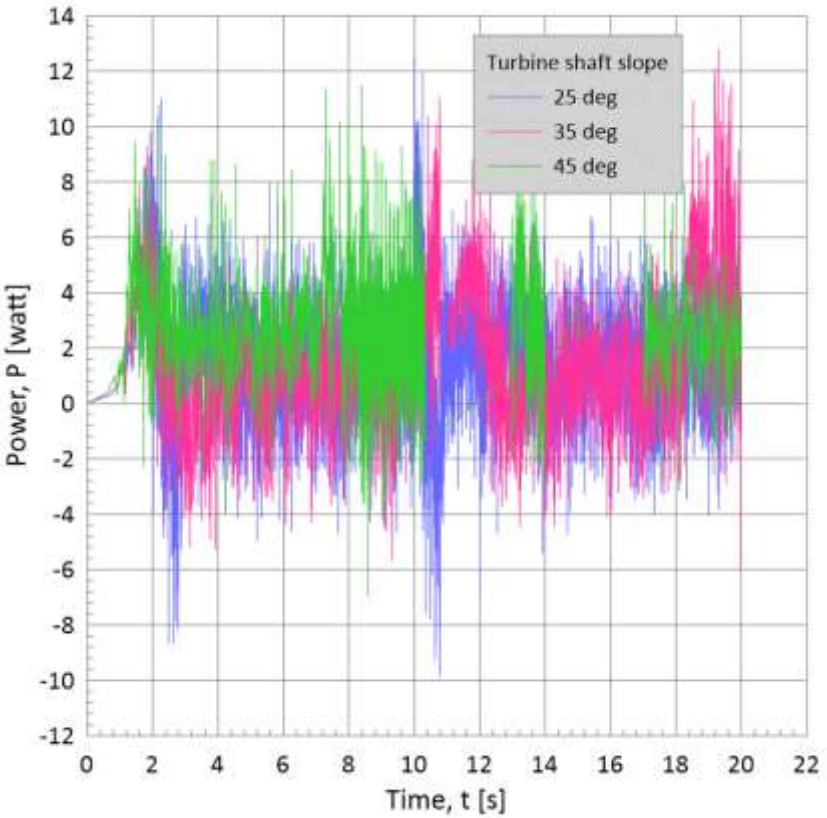

Figure 15. Curves transient of power with slope 25º, 35º and 45º.

BAB 5
PRESSURE

After the explicit calculation of viscosity and gravity, pressure is calculated based on the particle placement. To calculate the pressure, from the particle number density after the explicit calculation, the following Poisson equation is solved by iterative calculation of the MPS method.

$$\nabla^2 p^{k+1} = \frac{\rho_{ij}}{\Delta t^2} \frac{n^* - n^0}{n^0} \tag{58}$$

Particleworks employs the following equation, which is created by including compressibility α and a relaxation coefficient for stabilization λ_{rat} in the above equation.

$$\nabla^2 p^{k+1} = -\lambda_{rat} \frac{\rho_{ij}}{\Delta t^2} \left(\frac{n^* - n^0}{n^0} - \alpha p^{k+1} \right) \tag{59}$$

In Particleworks the default values of the compressibility and relaxation coefficient are 10^{-9} and 0.2 respectively.

The Figures 16, 17 and 18 below shows the pressure flow calculation algorithm of the MPS method for screw turbine 25^o, 35^o and 45^o respectively

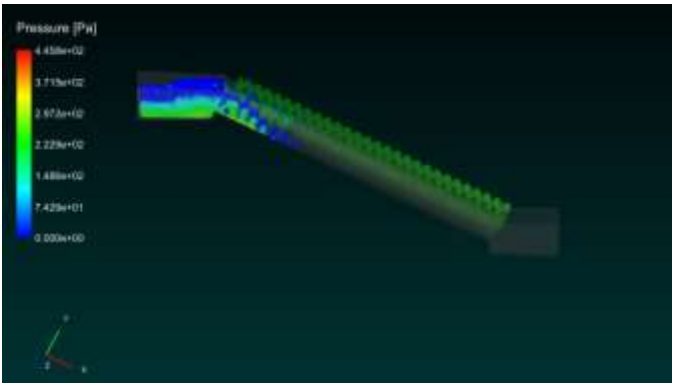

Figure 16.
Pressure distribution of transient of flow with slope 25º.

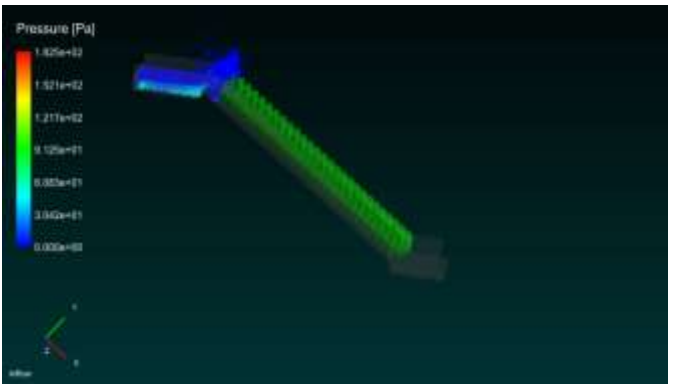

Figure 17.
Pressure distribution of transient of flow with slope 35º.

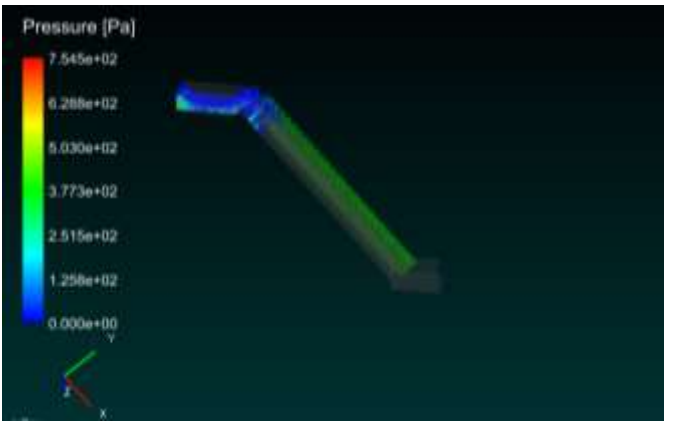

Figure 18.
Pressure distribution of transient of flow with slope 45º.

BAB 6
VELOCITY

From the calculated pressure, the pressure gradient is found, and the velocity is corrected by the following equations:

$$\vec{u}_i^{'} = -\frac{\Delta t}{\rho_i}\nabla p^{k+1} \tag{60}$$

Velocity and position correction by the pressure gradient

$$\frac{\vec{u}^{k+1} - \vec{u}^{*}}{\Delta t} = -\frac{\nabla p^{k+1}}{\rho} \tag{61}$$

The Figures 19, 20 and 21 below shows the velocity flow calculation algorithm of the MPS method for screw turbine 25^{o}, 35^{o} and 45^{o} respectively

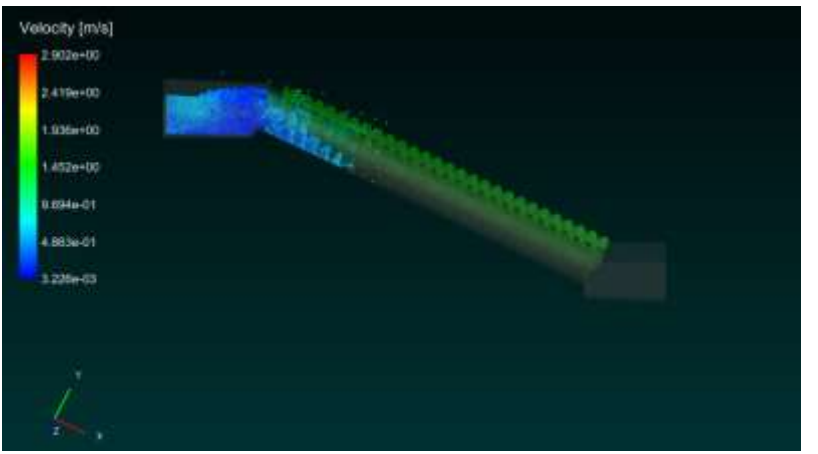

Figure 19.
Velocity distribution of transient of flow with slope 25^{o}.

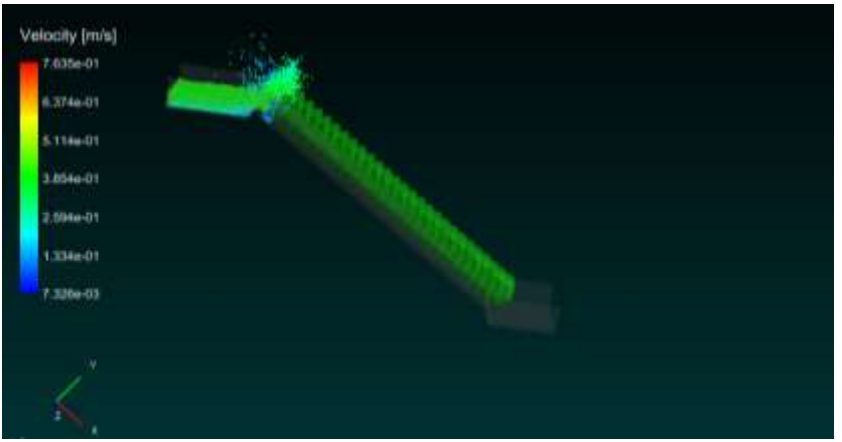

Figure 20.
Velocity distribution of transient of flow with slope 35º.

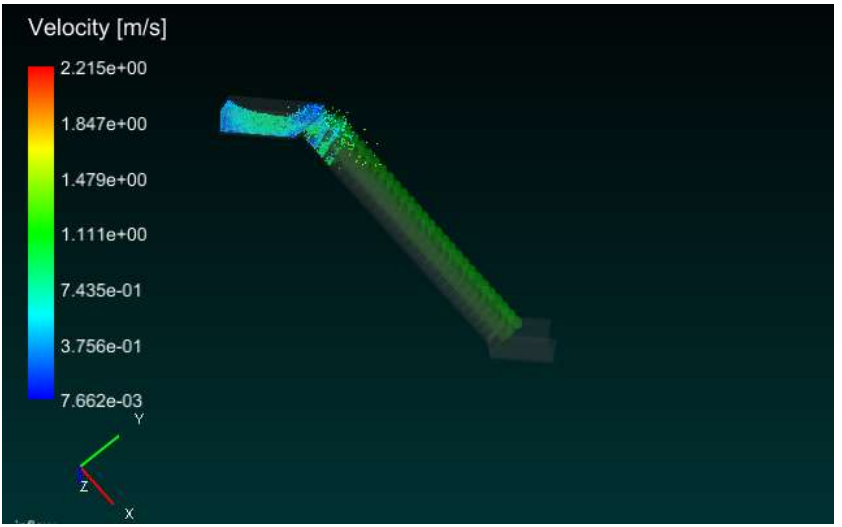

Figure 21. Velocity distribution of transient of flow with slope 45º.

The Figures 22, 23 and 24 below shows the streamlines flow calculation algorithm of the MPS method for screw turbine 25º, 35º and 45º respectively

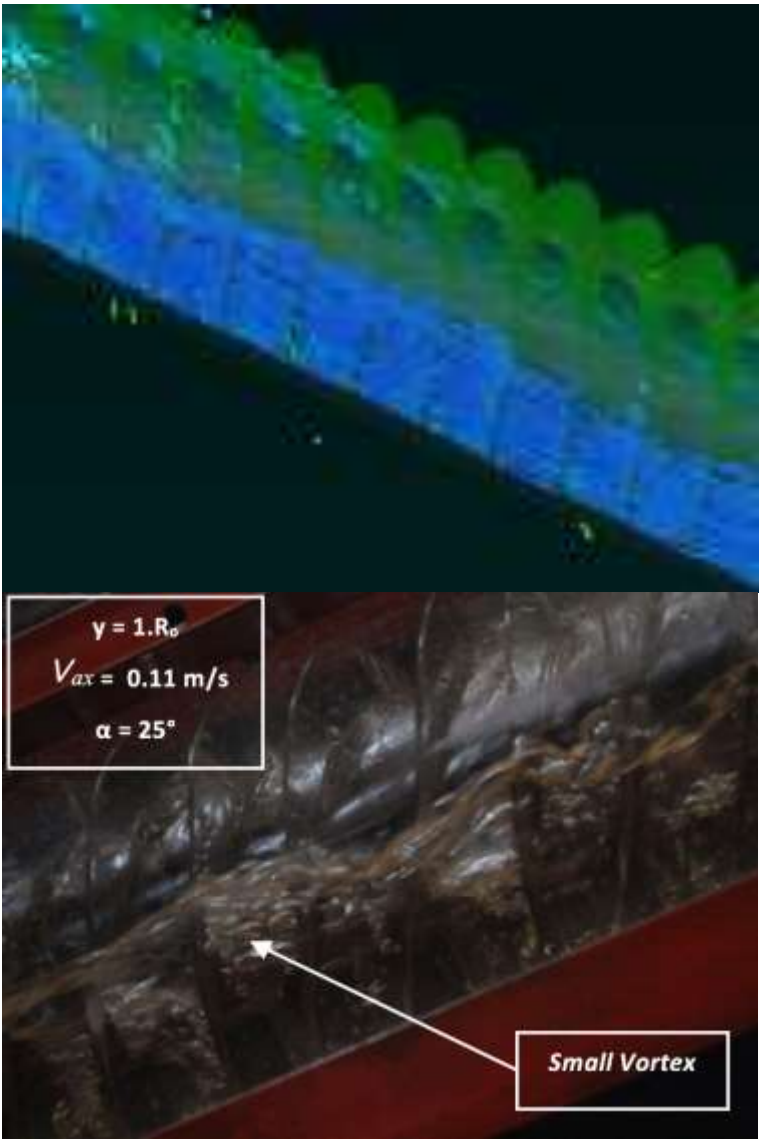

Figure 22. Streamlines velocity of transient of flow with slope 25º (right [7])

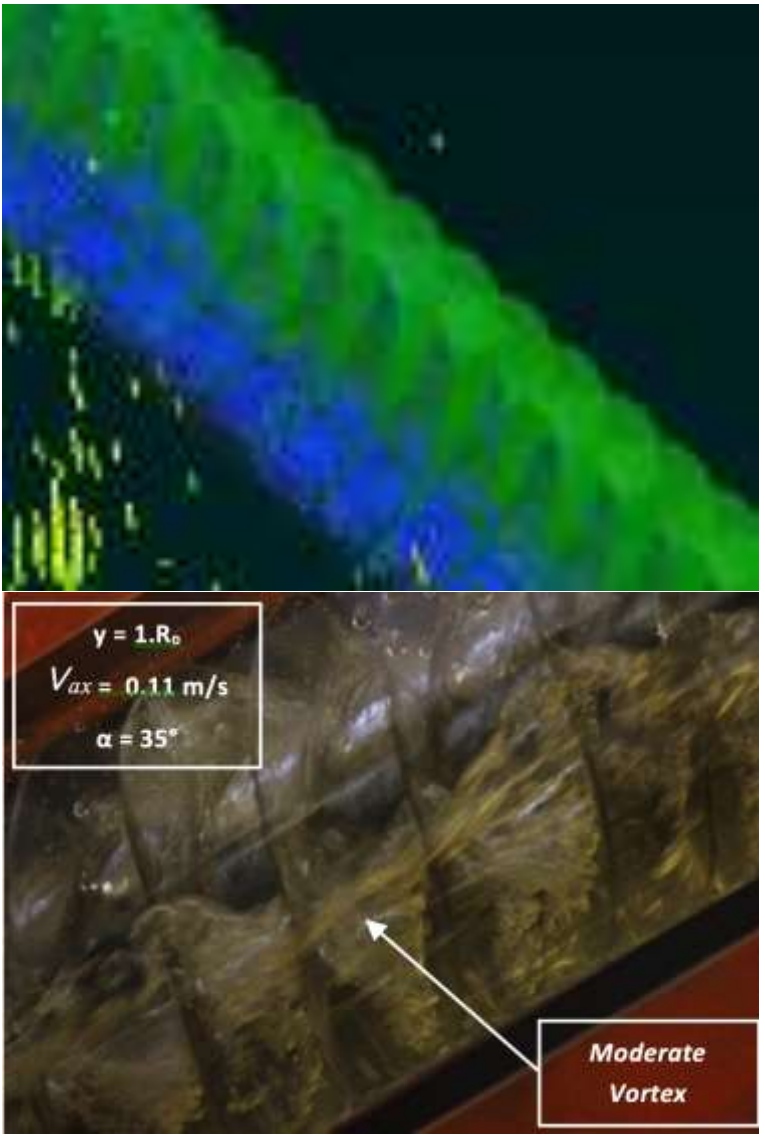

Figure 23. Streamlines velocity of transient of flow with slope 35º (right [7])

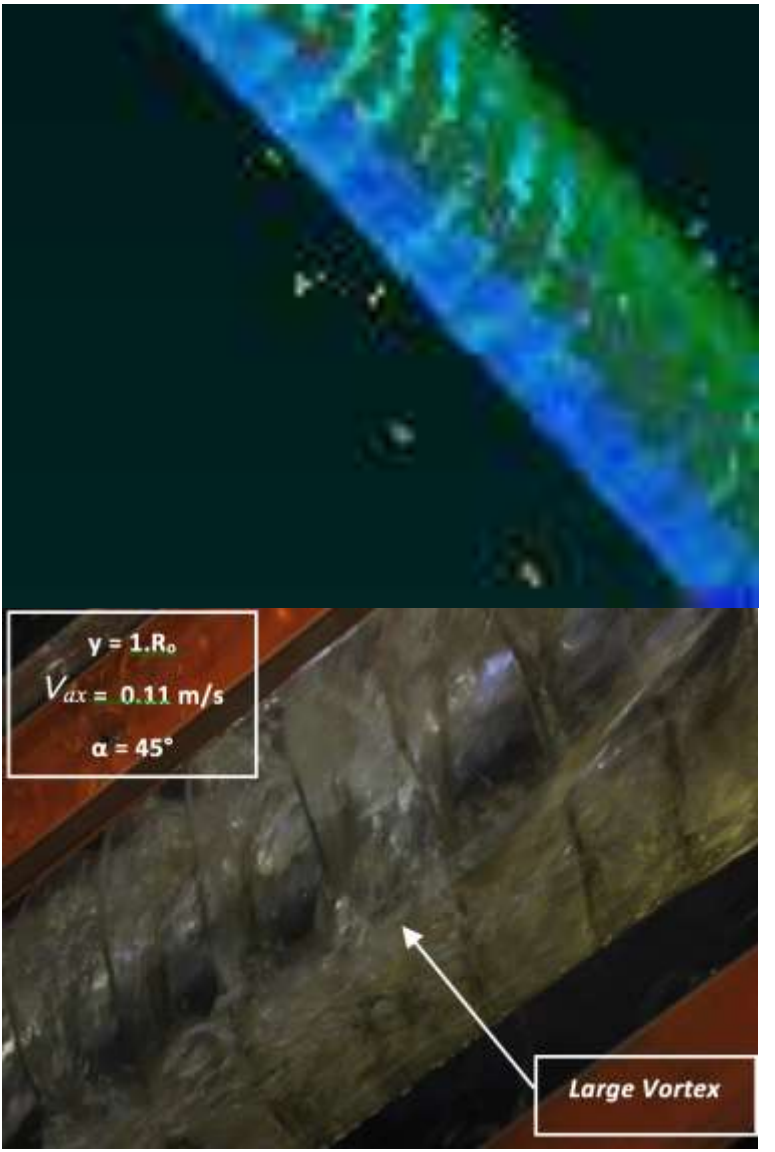

Figure 24. Streamlines velocity of transient of flow with slope 45º (right [7])

BAB 7
FREE SURFACE

The Figures 25, 26 and 27 below shows the free surface flow calculation algorithm of the MPS method for screw turbine 25^{o}, 35^{o} and 45^{o} respectively

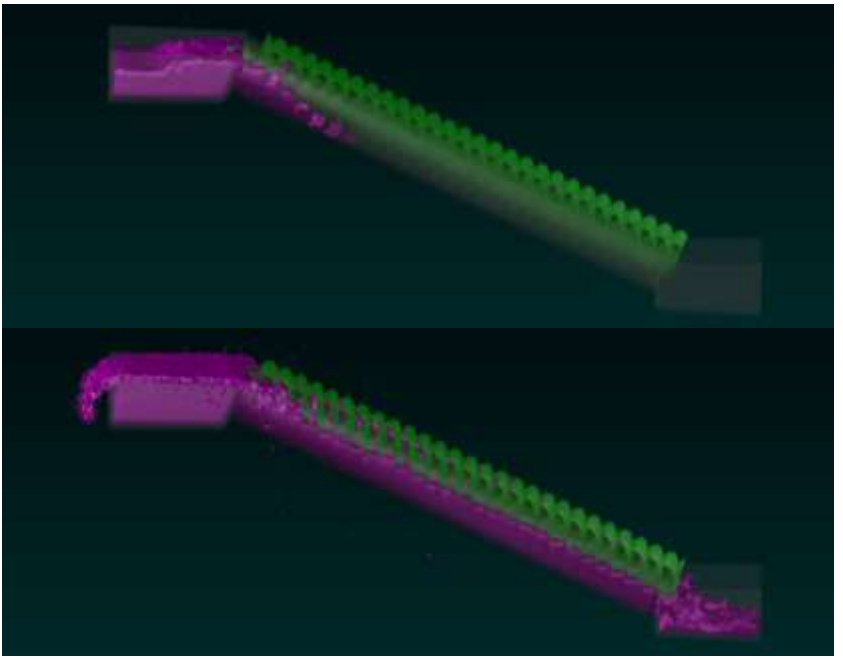

Figure 25. Free surface of transient of flow with slope 25^{o}

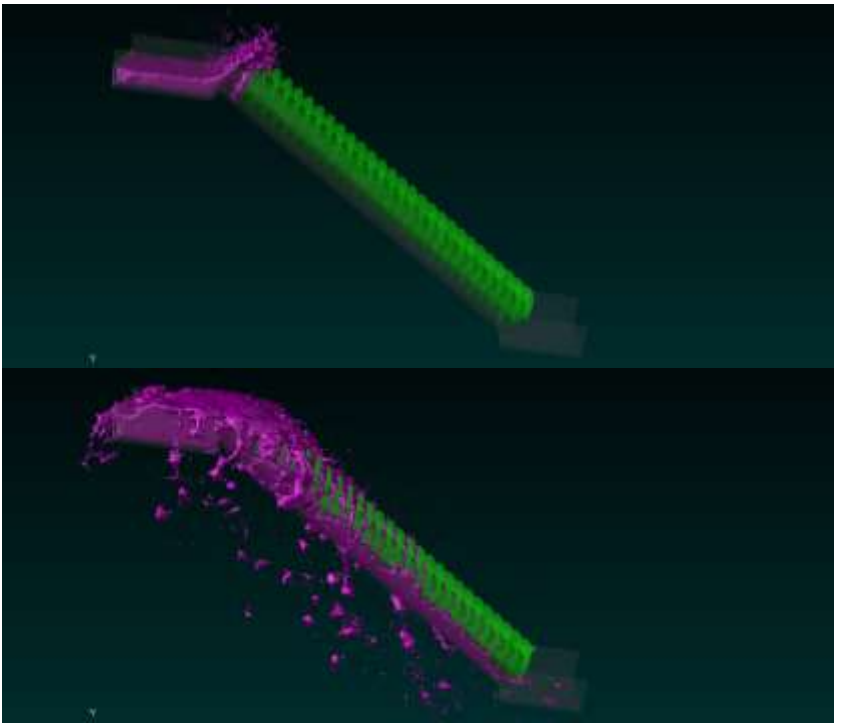

Figure 26. Free surface of transient of flow with slope 35º

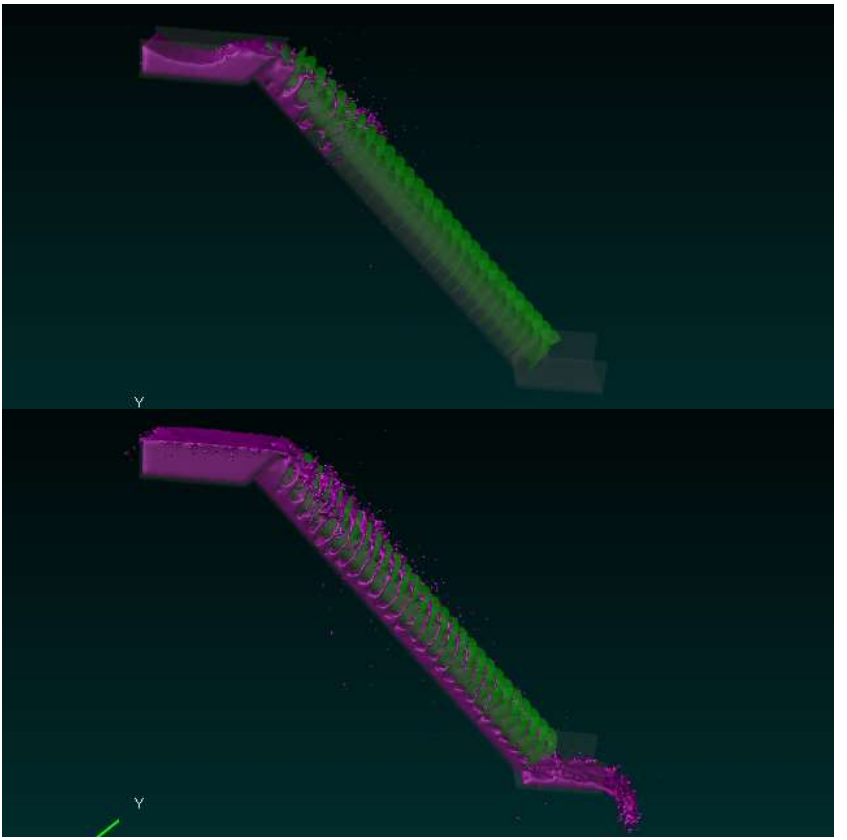

Figure 27. Free surface of transient of flow with slope 45º

BAB 8
TURBINE POWER

Based on the average value of the angular speed curve (figure 13), torque curve (figure 14) and turbine power (figure 15) at each turbine slope angle from the simulation results and compared with the test results [7], a comparison curve of the simulation results with the test results is shown. in Figures 28, 29 and 30 respectively. Specifically, the turbine power curve shows the available water potential at a certain elevation/head, so that the turbine efficiency value can be calculated based on equation (3) and the turbine efficiency curve is shown in Figure 31.

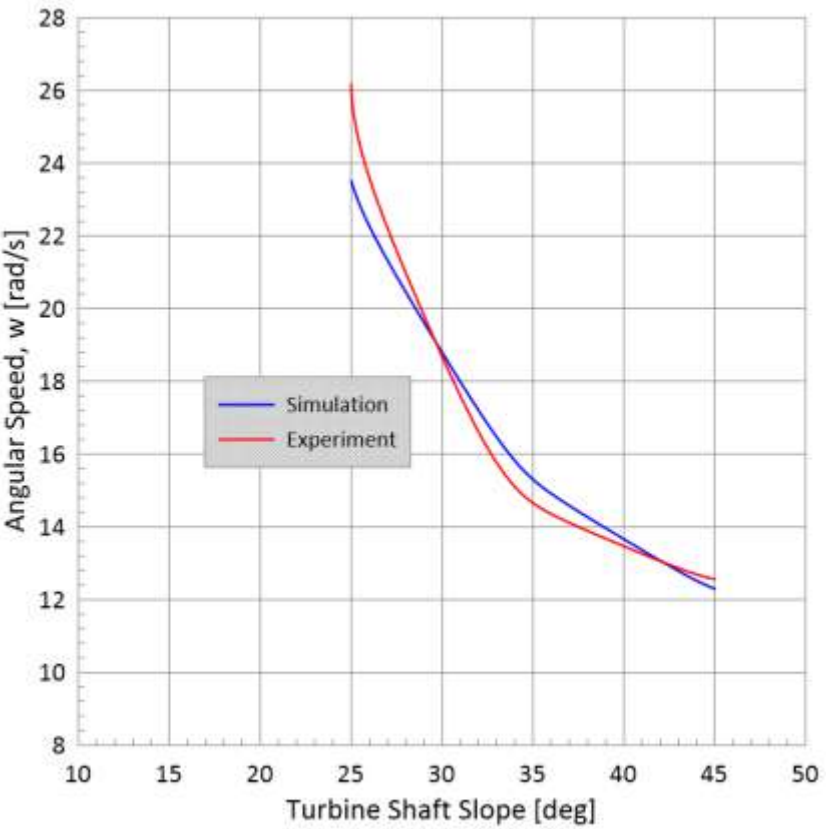

Figure 28. Curves of angular speed to turbine shaft slope

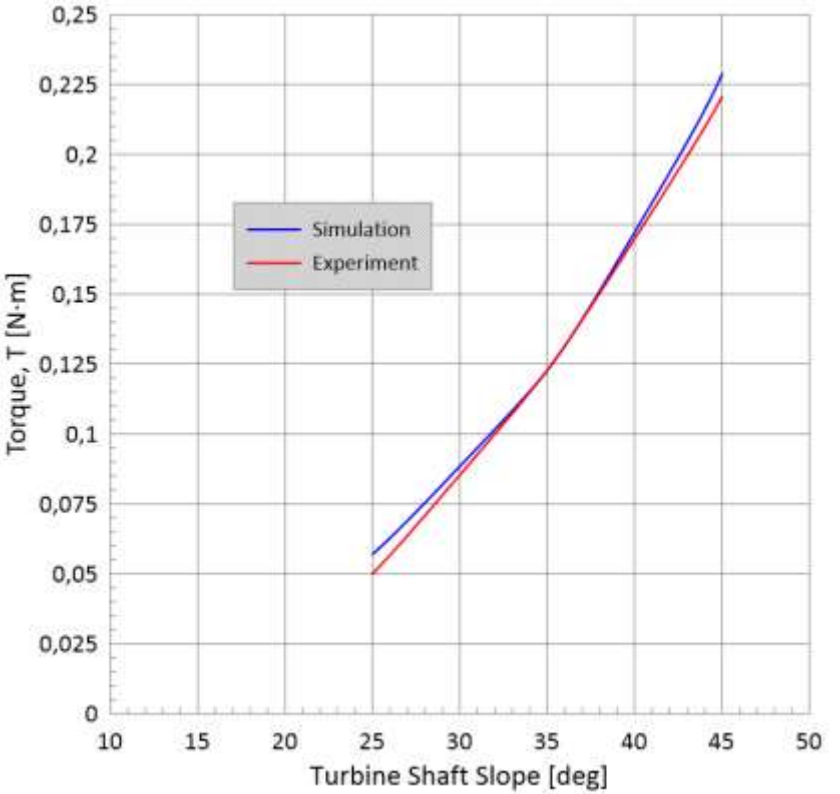

Figure 29. Curves of torque to turbine shaft slope

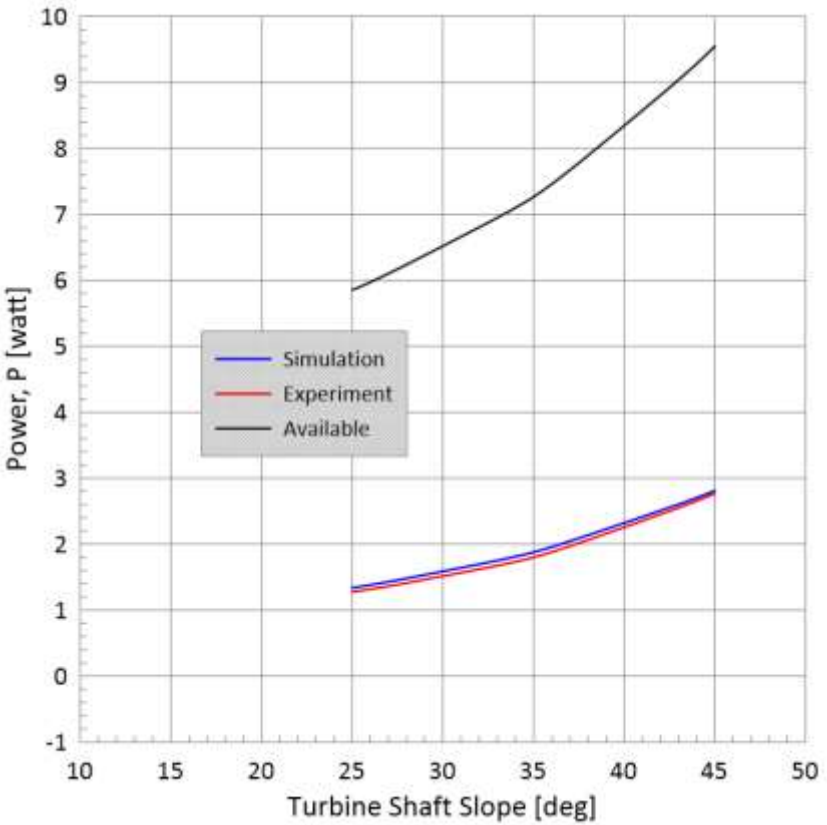

Figure 30. Curves of power to turbine shaft slope

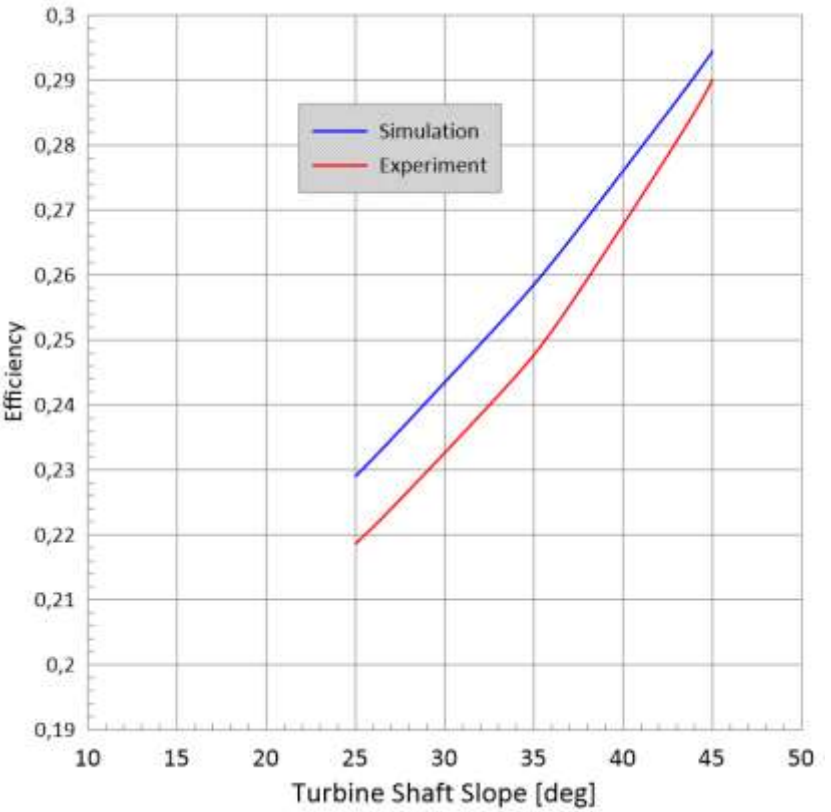

Figure 31. Curves of efficiency to turbine shaft slope

REFERENCES

[1]. David Kilama Okot, 2013. “Review of Small Hydropower Technology” Journal of Renewable and Sustainable Energy Reviews, Vol. 26 pp. 515- 520, Elsevier.

[2]. Elbatran A.H, et al., 2015. “Operation, Performance and Economic Analysis of Low Head Micro-Hydropower Turbines for Rural and Remote Areas: A Review” Journal Renewable and Sustainable Energy Reviews, Vol. 43, pp. 40-50. Elsevier.

[3]. Müeller. G. 2009. “Simplified Theory of Archimedean Screw”, Journal of Hydraulic. Vol. 47, pp. 666-669, University of Southampton, UK.

[4]. Rorres, C. 2000. “The Turnoff the Screw: Optimal Design of the Archimedean Screws”, Journal of Hydraulic, 126(1), 72-80.

[5]. Nuembergk Dirk. M. and Chris Rorres, 2013 “Analytical Model for Water Inflow of an Archimedes Screw Used in Hydropower Generation” Journal of Hydraulic Engineering, vol. 139, no. 2

[6]. Tineke Saroinsong, Rudy Soenoko, Slamet Wahyudi1, Mega Nur Sasongko, 2015, “The Effect of Head Inflow and Turbine Axis Angle Towards The Three Row Bladed Screw Turbine Efficiency”, International Journal of Applied Engineering Research, ISSN 0973-4562 Volume 10, Number 7 (2015) pp. 16977-16984.

[7]. Tineke Saroinsong, Rudy Soenoko, Slamet Wahyudi and Mega N Sasongko, 2016, “Fluid Flow Phenomenon in a Three-Bladed Power-Generating Archimedes Screw Turbine”, Journal of Engineering Science and Technology Review 9 (2) (2016) 72-79.

[8]. Reza Ali, et al. 2013. “Modeling of Archimedes Turbine for Low Head Hydro Power Plant in Simulink MATLAB” International Journal of Engineering Research & Technology, Vol. 2 Issue 7.

[9]. Scott Simmons, 2018, “A Computational Fluid Dynamic Analysis of Archimedes Screw Generators”, Thesis of The University of Guelph, Ontario, Canada.

[10]. Omar Sulaiman Abdullah, Wissam Hashim Khalil, Ammar Hatem Kamel, Amir J. Shareef, 2020, “Investigation of

Physical and Numerical Model of Archimedes Screw Turbine", Journal of Power and Energy Engineering, 2020, 8, 26-42, Scientific Research Publishing Inc.

[11]. Francesc Xavier Espinosa Vila, 2019, "CFD Simulations of An Archimedes Screw", Thesis, Mechanical Engineering, Ostbayerische Technische Hochschule Regensburg, Germany

[12]. Dylan Sheneth Edirisinghe, Ho-Seong Yang, Min-Sung Kim 1, Byung-Ha Kim 1, Sudath Prasanna Gunawardane and Young-Ho Lee, 2021, "Computational Flow Analysis on a Real Scale Run-of-River Archimedes Screw Turbine with a High Incline Angle", Energies Journal, 2021, 14, 3307, MDPI, Basel, Switzerland

[13]. Alkistis Stergiopoulou, Vassilios Stergiopoulos, 2021, "CFD Simulations of Tubular Archimedean Screw Turbines Harnessing the Small Hydropotential of Greek Watercourses", International Journal of Energy and Environment, Volume 12, Issue 1, 2021 pp.19-30

[14]. C. W. Hirt and B. D. Nichols, 1981, “Volume of fluid (VOF) method for the dynamics of free boundaries,” J. Comput. Phys. 39, 201–225.

[15]. M. Sussman, P. Smereka, and S. Osher, 1994, “A level set approach for computing solutions to incompressible two-phase flow,” J. Comput. Phys. 114, 146–159.

[16]. 3C. H. Hu and M. Kashiwagi, 2004, “A CIP-based method for numerical simulations of violent free-surface flows,” J. Mar. Sci. Technol. 9, 143–157.

[17]. S. Koshizuka and Y. Oka, 1996, “Moving-particle semi-implicit method for fragmentation of incompressible fluid,” Nucl. Sci. Eng. 123, 421–434.

[18]. R. A. Gingold and J. J. Monaghan, 1977, “Smoothed particle hydrodynamics: Theory and application to non-spherical stars,” Mon. Not. R. Astron. Soc. 181, 375–389.

[19]. L. B. Lucy, 1977, “A numerical approach to the testing of the fission hypothesis,” Astron. J. 82(12), 1013–1024.

[20]. S. R. Idelsohn, E. Oñate, and F. D. Pin, 2004, “The particle finite element method: A powerful tool to solve

incompressible flows with free-surfaces and breaking waves," Int. J. Numer. Methods Eng. 61(7), 964–989.

[21]. L. Imas, J. Grant, D. Kring, and W. M. Milewski, 2003, "Investigation of freesurface flow in the near-field of an advancing surface-piercing body using threedimensional smoothed particle hydrodynamics," in Proceedings of the International Conference on Numerical Ship Hydrodynamics (Association for Computing Machinery), pp. 340–349.

[22]. 16K. Iida and H. Akimoto, 2003, "Two- and three-dimensional CFD simulations of a planing body by a particle method," in Ninth Symposium on Nonlinear and Free-Surface Flows (Hiroshima University), pp. 75–78.

[23]. Colagrossi and M. Landrini, 2003, "Numerical simulation of interfacial flows by smoothed particle hydrodynamics," J. Comput. Phys. 191(2), 448–475.

[24]. M. Sueyoshi, M. Kashiwagi, and S. Naito, 2008, "Numerical simulation of waveinduced nonlinear motions of a two-dimensional floating body by the moving particle semi-implicit method," J. Mar. Sci. Technol. 13, 85–94.

[25]. K. Shibata, S. Koshizuka, and K. Tanizawa, 2009, “Three-dimensional numerical analysis of shipping water onto a moving ship using a particle method,” J. Mar. Sci. Technol. 14, 214–227.

[26]. H. Akimoto, 2003, “Numerical simulation of the flow around a planing body by MPS method,” Ocean Eng. 64, 72–79.

[27]. 21A. Dashtimanesh and P. Ghadimi, 2013, “A three-dimensional SPH model for detailed study of free surface deformation, just behind a rectangular planing hull,” J. Braz. Soc. Mech. Sci. Eng. 35, 369–380.

[28]. Çengel, Y.A. and Cimbala, J.M., 2006, “Fluid Mechanics: Fundamentals and Applications”, Mc-Graw-Hill, New York.

[29]. Prometech Software, Inc, 2016, “Theory Manual Release 6.0.0”,

[30]. CholJun Pak, PokNam Han, KwangChol Ri, YongKwang Ri, and InChol Hwang, 2021, “Numerical analysis of the nonlinear free surface flow around an advancing ship using

moving particle semi-implicit method", AIP Advances 11, 035106 (2021); doi: 10.1063/5.0039016.

[31]. Carlos Andrés Pérez Gutiérrez, 2016, "Implementation of the Moving Particle Semi-implicit method to predict the drag resistance coefficient on 2D", PhD thesis, Facultad de Ingeniería Universidad Eafit Medellín.